Hindawi
Advances in Materials Science and Engineering
Volume 2018, Article ID 4730192, 7 pages
https://doi.org/10.1155/2018/4730192

Research Article

Carbon Nanoparticle-Supported Pd Obtained by Solar Physical Vapor Deposition

Alexandru Pascu, Elena Manuela Stanciu, Cătălin Croitoru, Ionut Claudiu Roată, and Mircea Horia Tierean

Materials Engineering and Welding Department, Transilvania University of Brasov, 29 Eroilor, Brasov 500036, Romania

Correspondence should be addressed to Cătălin Croitoru; c.croitoru@unitbv.ro

Received 31 August 2017; Revised 14 November 2017; Accepted 6 December 2017; Published 15 February 2018

Academic Editor: Mikhael Bechelany

Palladium supported on carbon nanoparticles has been obtained on a specially designed ceramic catalyst, obtained by thermal spraying on a copper substrate, starting from Pd/C targets. Solar physical vapor deposition in argon, an environment-friendly and energy-efficient alternative to arc or chemical vapor deposition, has been employed as a means of target vaporization at CNRS-PROMES facility in Odeillo, France. The obtained nanoparticles have a spherical-porous morphology with diameters ranging from 50 to 120 nm and specific sorption areas of 50,000 m^2/g. The XRD diffractograms indicate the presence of dominatingly crystalline short-range ordered graphene oxide layers, in contrast with the amorphous Pd/C starting precursor. The presence of palladium (0.6% wt.) at the surface of the nanoparticles was proved by the EDX and XRD analyses, making the synthesized material useful in applications such as catalysis or gas sorption.

1. Introduction

The optimization of industrially important technological processes and the devising of greener and cost-efficient methods have led to an increase in the search for alternative energy sources and better materials in the last decade [1]. Palladium is one of the most widely used metal catalysts in the chemical industry. It is often used as a support for hydrogenation reactions [1, 2], as a catalyst for oxidation [3] or disproportionation reactions [4], as an electrocatalyst for fuel cells [5], for gas sorption purposes [6], and so forth. Its efficiency is enhanced when dispersed on a substrate with an increased surface area, among which carbon-based supports are the most widely employed [7]. To further increase the specific surface area in catalysis reactions, various nanoscale carbonaceous-shaped supports have been recently employed as substrates for palladium, among which could be noted carbon nanoparticles [8], nanofibers [9], hollow nanospheres [10], or nanotubes [1, 11]. Usually, a three-step "wet" synthesis of nanoscale carbon-supported Pd is employed [1, 9–11]. Firstly, the nanomaterial is obtained by chemical vapor deposition, arc deposition, or physical vapor deposition, onto which Pd^{2+} ions (as such, or as complexes) are adsorbed, followed by the chemical or electrochemical reduction of Pd^{2+} to metallic Pd [11]. The use of potentially harmful volatile organic compounds, such as aldehydes or volatile solvents, and the tedious separation of the resulted material from the liquid phase as well as its purification (from the surfactants, oxidized reducing agents) represent an impediment in industrial application of nanoscale supported Pd. Various green processes used up to date involve the use of milder reducing agents or surfactants for Pd^{2+} (plant extracts derived) [12, 13] but with reduced application potential at industrial scale.

The aim of this paper is to obtain palladium supported on carbon nanoparticles in a one-step time- and economic-efficient process, by using the solar physical vapor deposition (SPVD) technique, starting from a target of 10% Pd on active carbon. For nucleation and growth of palladium supported on carbon nanoparticles (Pd/NPs), a custom catalyst has been obtained by thermal spraying of an Al_2O_3-TiO_2-hydroxyapatite mixture, which composition was perfected in our earlier

studies [14]. The SPVD technique, employed in "heliotron" solar reactors through the infrastructure present at CNRS-PROMES facility in Odeillo-Font Romeu, France [15], has been already used up to date to obtain metal oxide nanoparticles (TiO_2 polymorphs [16], ZnO, ZrO_2, or mixt oxides [17]), and ceramic nanoparticles (titanates and zirconates) [18]. A limited amount of data is reported on carbonaceous nanomaterials' synthesis through SPVD [15, 19, 20], and up to our knowledge no reports exist up to date concerning the synthesis of palladium-containing nanomaterials through this method.

The cost-efficiency of SPVD through using concentrated solar radiation, as well as through devising Pd-loaded nanoparticles with high surface area in a one-step synthesis approach, could lead to a more rapid implementation of nanoparticulated Pd/C in the chemical industry, thus aiding to create a more sustainable society and environment.

2. Materials and Methods

2.1. Materials. Palladium 10 wt.% loading, supported on activated carbon (Sigma Aldrich), has been pelted by means of a hydraulic press in cylindrical targets (10 mm diameter and 3 mm thickness).

The catalyst for SPVD-assisted nanoparticle nucleation and growth has been obtained by flame spraying on pure copper (CastoDyn DS8000 oxy-acetylene thermal spray system) of a ceramic mixture comprised in Al_2O_3 : TiO_2 : hydroxyapatite (HA) (57% : 38% : 5% wt.). The spraying gun-substrate distance was 200 mm, the copper support rotation speed was of 127 rpm, and the powder feed rate was 15 g/min. The custom catalyst composition has been optimized in our previous research [14], to obtain a good adherence to the copper substrate and to enhance the formation of several mixed oxide phases such as $CaCu_3Ti_4O_{12}$ and titanates ($CaTiO_3$) which enhance the nanoparticles growth, as determined from the previous XRD analysis results of the catalyst surface [21].

2.2. SPVD Process of Pd/NP Obtaining. The experimental tests regarding the solar physical vapor deposition were carried out at CNRS-PROMES solar research facility, Font Romeu, France, using a 2 kW vertical solar furnace containing a spherical glass reactor.

The spherical Pyrex "heliotron" glass reactor is formed mainly of two parts: (1) a water-cooled metallic support onto which the cylindrical-shaped thermal-sprayed catalyst support is clamped, placed at the top of the reactor and (2) a water-cooled copper support for the Pd/C target, situated at the base of the glass reactor. Both pieces are hermetically clamped on the glass. On the superior part of the reactor could be found an inlet for inert gas admission and an outlet for the vacuum (6) (general overview of the whole reactor installation is presented in Figure 1(a)).

Above the reactor, a parabolic mirror is placed, which concentrates the solar radiation on the Pd/C target (target vaporization could be observed in Figure 1(b)), aiding in the formation of the gaseous ionic Pd and C plume which condenses on the colder part of the reactor (the water-cooled ceramic catalyst). Further details on the outlook and functioning of the installation could be found in other research, such as that described by Flamant et al. [15], Apostol et al. [18], and Stanciu et al. [21].

The overall aspect of the catalyst after deposition of Pd/NP is illustrated in Figure 1(c). The total reaction time (Pd/C target vaporization and NP nucleation and growth) has been 10 min, optimized during prior experimental trials [21], considering the avoiding of catalyst "supersaturation" and carbon deposition on the glass walls of the reactor, occurring at reaction times longer than 10 minutes, which could cause the fracturing of the glass reactor. The pressure inside the reactor has been kept at 225 mmHg, and the argon flow rate was 0.35 L/min. Three experimental batches have been obtained for this experimental setup, and the NPs have been collected avoiding their contamination. For a single experiment, an overall efficiency of 7.5% has been reached, considering the operational parameters of the SPVD process. For lower reaction times, the amount of collected material was insufficient for performing the structural analysis, so it has been considered that 10 minutes reaction time was optimal for this experimental setup.

2.3. Pd/NP Characterization. The overall scanning electron microscopy images of the catalyst surface and cross section after Pd/NP deposition and in-depth morphology of the Pd/NP collected from the catalyst surface have been attained with a Hitachi SU5000 field-emission scanning electron microscope after placement on a silicon wafer and gold sputtering (average thickness of gold film of 45 nm) and with a FEI/Philips EM 208 S transmission electron microscope (NPs deposited on a 300 mesh PELCO copper grid). The elemental weight percent of the Pd/NPs has been determined through the energy-dispersive X-ray (EDX) spectroscopy of the SEM microscope, prior to gold sputtering.

The XRD diffractograms of the Pd/C target and of the obtained Pd supported on carbon nanoparticles were obtained with an Advanced D8 Discover Bruker diffractometer, at Cu-Kα1 = 1.5406 Å wavelength, 40 kW, 20 mA, scan speed of 2°/min, and 2θ range from 10 to 70°.

3. Results and Discussion

As it could be seen in Figures 1(b) and 2(a), the deposition of carbonaceous nanomaterial on the ceramic catalyst has been reached. Due to differences in electron reflectivity of the materials, the Pd/NPs appear as white, aggregated deposits (Figure 2(b)) unevenly distributed on the ceramic substrate catalyst. This uneven distribution on the catalyst surface could be due to differences in the surface Gibbs potential (ΔG) of the ceramic catalyst phases. Nucleation occurs on the phases with the highest ΔG values, as found in other research [22, 23].

It could be seen from Figure 2(b) that high-electron beam reflectivity areas (whiter areas) are located mainly on the palladium nanoparticle aggregates. Palladium metal presents high reflectivity for the electron beam. The cross-sectional SEM micrographs of the as-deposited catalyst show an average thickness of the Pd/NP layer of 0.75 μm.

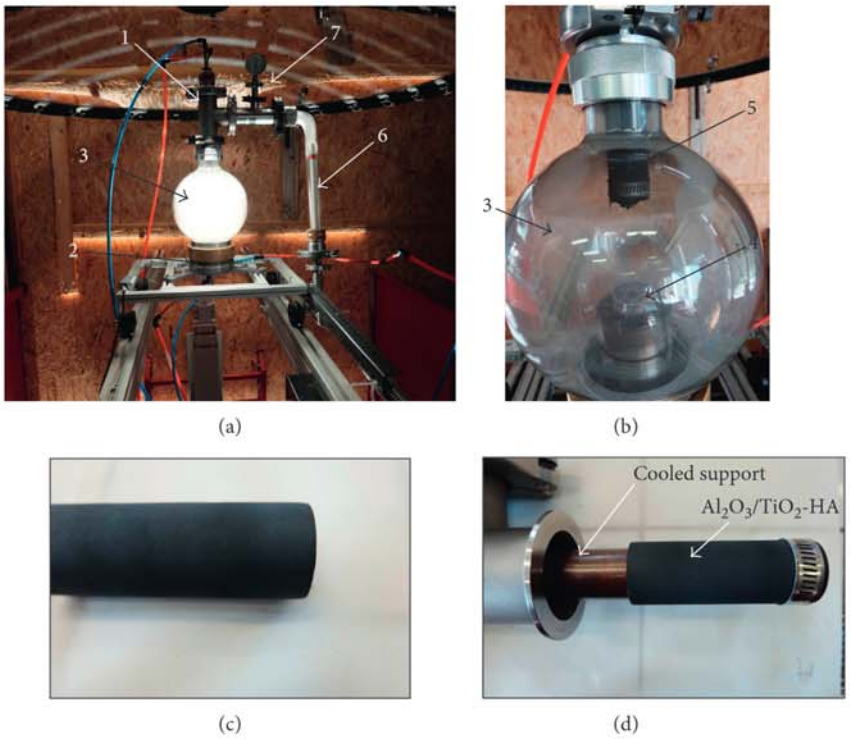

Figure 1: (a) Experimental setup used for the solar synthesis of palladium-doped carbon nanoparticles; (b) detail of the solar reactor; (c, d) ceramic-metallic catalyst. (1) Water-cooled system of the ceramic catalyst, (2) water-cooled support for the Pd/C target, (3) Pyrex glass reactor, (4) target positioned on the cooled support, (5) catalyst, (6) vacuum extraction and ceramic filter, and (7) manometer.

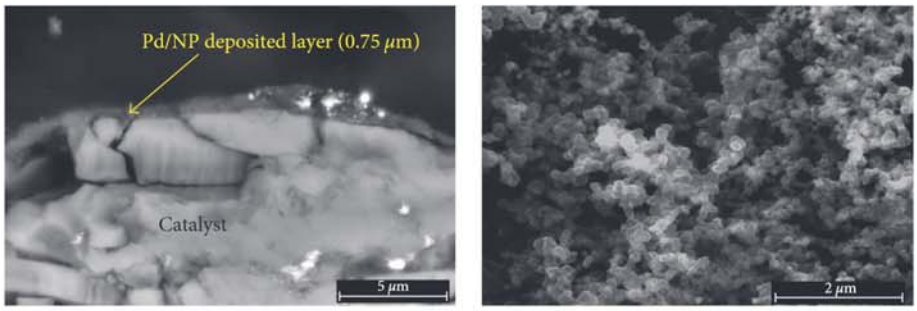

Figure 2: (a) Catalyst cross section after Pd/NP deposition; (b) Pd/NP deposited on the catalyst surface (after gold sputtering).

The Pd/NP EDX analysis of the elemental content confirms the presence of palladium with a weight percent of 0.6, which reported that the amount of carbon in the sample is 2.4% wt. (Figure 3). This lower amount of Pd on the surface of the SPVD-deposited material, comparing to the initial Pd loading in the activated carbon/Pd target, could be owed to the lower vaporization enthalpy of Pd (358 kJ/mol) [24] comparing to that of carbon to gaseous carbon species (452.69 kJ/mol) [25]. In this respect, the thermodynamically facilitated vaporization of palladium generates deposits on the surface of the catalyst, which are further covered by the condensing carbonaceous species.

As the complete elimination of oxygen from the installation could not be achieved in this setup, the vacuum could not be increased further due to safety reasons related to the glass reactor, and a mild oxidation of the material's surface has been noted, as confirmed also by the XRD data (the presence of graphene oxide, Figure 7). The presence of oxygen could increase the hydrophilic nature of the nanoparticles surface, which could be useful in some applications, such as catalysts for hydrogenation reactions (i.e., in the case of carbonyl compounds). The determined oxygen content (42.5%) is comparable to other research [25]. The presence of Na, Mg, and Si on the surface of the nanoparticles could be due to impurification from the contact with the SPVD catalyst layer. No detectible amount of Ti and Al was recorded, although Ca and P (from hydroxyapatite) were present in a significant percent on the surface of the nanoparticles.

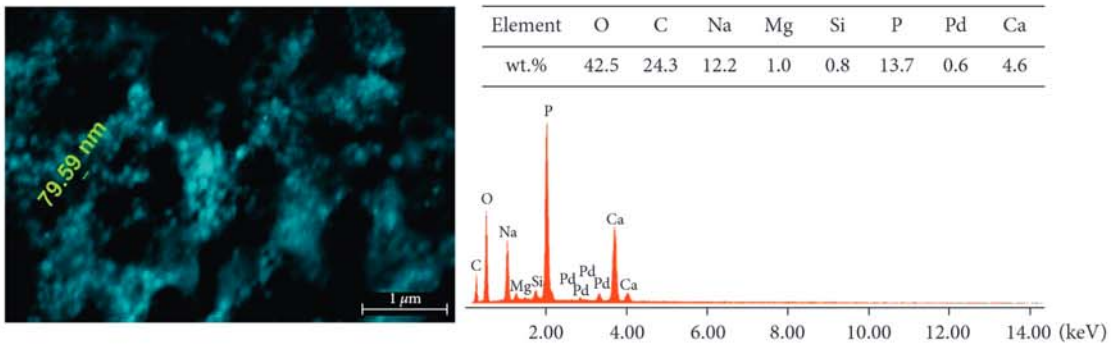

Figure 3: High-contrast SEM image and EDX analysis of the surface of Pd/NPs.

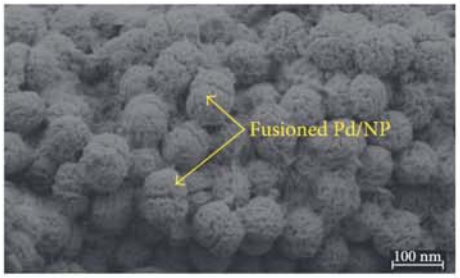

(a)

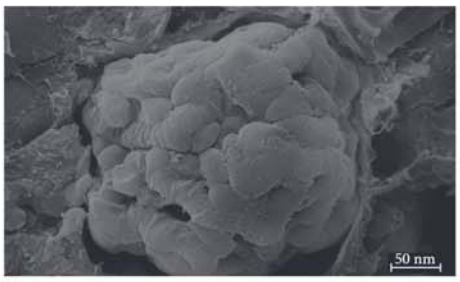

(b)

Figure 4: (a) FE-SEM of Pd/NPs deposit on the surface of the ceramic catalyst; (b) detail on a single Pd/NP.

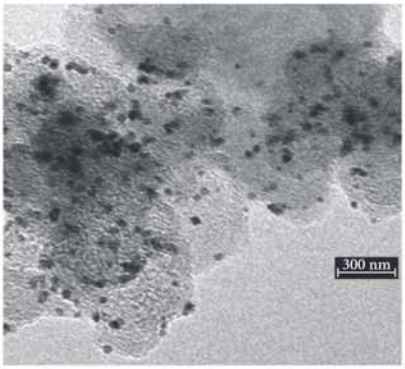

(a)

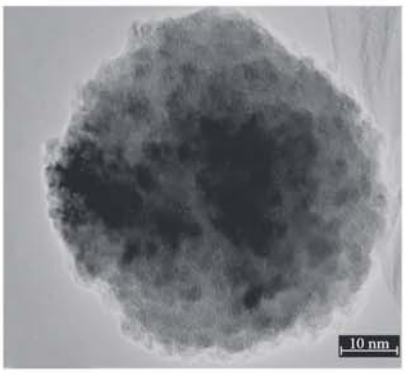

(b)

Figure 5: TEM micrographs of the collected Pd/NPs.

Field-emission SEM (FE-SEM) micrographs of a catalyst region rich in NP deposits (Figure 4(a)) reveal further insight into the morphology of the carbon nanoparticle-supported Pd. These present an irregular spherical morphology, with diameters in the 50–120 nm range, like those of readily available commercial carbon nanoparticles [10].

The employed synthesis duration (10 minutes) determines a multilayer disposition of the Pd/NPs on the surface of the catalyst (roughly 6-5 layer, taking into account the thickness of the deposited layer and of the NP diameter distribution), determining the upper layers of nanoparticle nucleation and growth on top of the previous ones. Due to this fact, in some areas, fusion of the Pd/NPs could be observed.

A FE-SEM micrograph of an individual Pd/NP is illustrated in Figure 4(b). The NP presents a "flower-bud" like appearance, as is usually typical for hydrothermal synthesis of inorganic nanomaterials [26] or carbon nanoparticles obtained by thermolysis [27]. The irregularities on the surface could be useful in catalytic applications, as they increase the active surface area of the nanoparticle. The BET nitrogen adsorption/desorption experiments indicate a pore average diameter of 5–10 nm, with an average BET surface area of 50,000 m^2/g, and a pore volume density of 0.51 cm^3/g (mass of NP samples taken into analysis was 0.080 g).

The spherical shape of the Pd/NPs is also confirmed by the TEM micrographs presented in Figure 5. Differences in electron transmission modes could be seen in the NPs, as deducted from the difference in contrast to the TEM micrographs of the NPs. This could be accounted for the presence of oxidized graphene sheets, which appears in

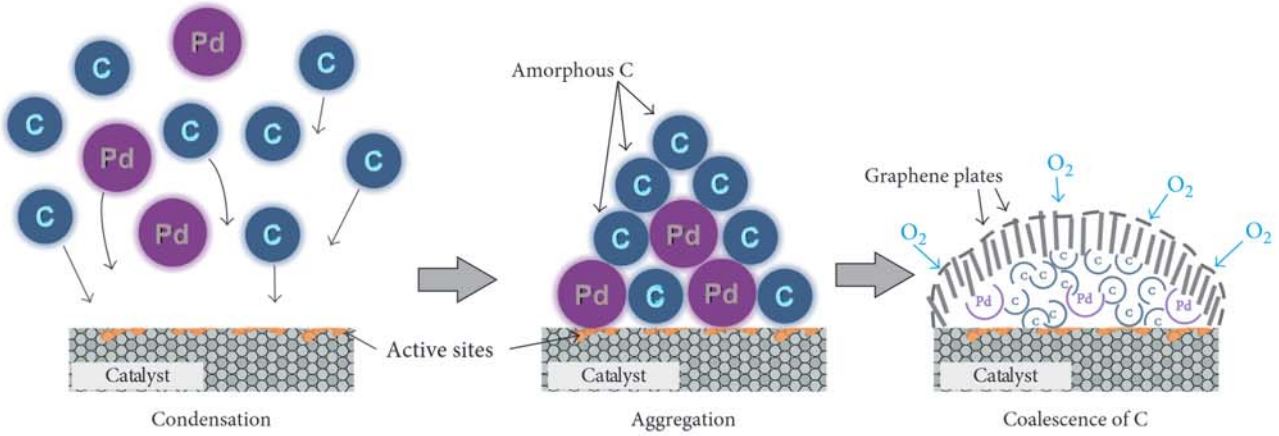

Figure 6: Principle mechanism of Pd/NPs formation.

a darker tone than the majority amorphous carbon matrix. As it has been determined in other research, the presence of metallic ions (such as Ca^{2+}) disrupts the fusion of gaseous carbonaceous species that form the graphene sheets [28]. The deposited palladium ions and the ionic species from the catalyst surface in this case act as disruptors for the crystallization of graphene in overstacked plates, contributing to the formation of a bulk, dominatingly amorphous carbonaceous matrix (lighter tone seen in the TEM micrograph from Figure 5) with spherical overall shape, according also to the principle mechanism proposed in Figure 6.

The XRD diffractograms of the obtained Pd/NPs and the Pd/C precursor target are presented in Figure 7.

The XRD diffractogram of the Pd/NPs presents a broad peak centered at 9.77° (full width at half maximum, as per (1), $\beta = 0.0311$ rad) usually found in graphene oxide [28]. Several other small diffraction peaks show the presence of palladium, in both metallic (Pd (111), peak centered at 39.68° [29], $\beta = 0.0157$ rad) and oxide forms (PdO, peak centered at 35.04° [30]). Comparing to the PdNPs, in the Pd/C target, the β value of the Pd (111) diffraction peak is 0.0036 rad. The diffractogram of Pd/NPs shows also a dominatingly crystalline matrix, possibly due to the presence of graphene oxide and trace rutile TiO_2 impurities from the ceramic catalyst (peak centered at 29.02°), in contrast with the Pd/C precursor target, which is dominatingly amorphous (broad diffraction peak at ~25°, ascribed to (002) diffraction plane of carbon [31]). Since the EDX results did not show the presence of Ti on the surface of the NPs and the XRD diffractogram evidenced the presence of rutile, there is little support as far as this introductory study is concerned, for the formation of mixt intermetallic phases such as $PdTi_2$. The formation of these phases, especially with TiO_2 as starting material, occurs at elevated temperatures (650 K and higher) [32] which are not reached on the catalyst surface since it is continuously water cooled.

The apparent crystallite sizes (L), for Pd, graphene oxide layers height and respective distance between layers for graphene oxide have been evaluated by the Scherrer equation (1), considering the full width at half maximum (β) of the representative diffraction peak for each phase taken into consideration [28, 33]:

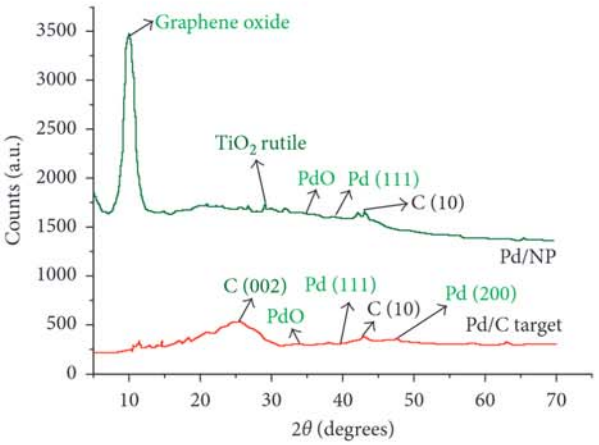

Figure 7: XRD diffractograms of the Pd/C target and of the Pd/NPs.

$$L = \frac{K \cdot \lambda}{\beta \cdot \cos\theta}, \quad (1)$$

where the Warren shape constant $K = 0.9$ for Pd and graphene layer height [33], and 1.84 for graphene layer distance evaluation [28], λ is the wavelength of the X-ray radiation, and θ is the Bragg angle of diffraction.

The apparent crystallite size for Pd (111) is 28.97 nm in the Pd/C target and 6.79 nm in the Pd/NPs. For the graphene oxide, considering the diffraction peak at 9.77°, the average distance between graphene layers is 8.96 nm, indicating a short-range order in their stacking. Considering the C (10) diffraction at ~43° ($\beta = 0.004$ rad) from the Pd/NP XRD spectrum, the average height of the graphene sheets is 24.82 nm, like other reported research [28].

4. Conclusions

In this paper, 10% Pd loaded on active carbon has been used as precursor material for the "green" synthesis of palladium supported on carbon nanoparticles. Physical vapor deposition using concentrated solar energy source has been used as a means of precursor vaporization and decomposition.

The optimized composition of the ceramic catalyst employed for nanoparticle nucleation and growth allowed the obtaining of spherical-shaped materials, with diameters in the 50–120 nm range, having high specific sorption area, namely, 50,000 m^2/g, with a narrow pore distribution between 5 and 10 nm. The X-ray diffraction analysis has indicated that the obtained nanoparticles contain a highly ordered graphene layer configuration, intercalated with amorphous carbon regions, generated by the "destructuration" effect of the palladium ions.

The results of this research could prove useful in designing new types of catalyst materials. Further studies will be dedicated to the testing of the catalysis efficiency of the obtained nanoparticles and to the testing of their sorption efficiency for various gasses (hydrogen, carbon oxides, and olefins). As the challenge for improving the cost-effectiveness of nanoscale catalysts, our approach in the synthesis of palladium supported on carbon could prove an economically viable alternative to other commercially available materials.

Conflicts of Interest

The authors declare that they have no conflicts of interest.

Acknowledgments

Financial support by the Access to Research Infrastructures activity in the 7th Framework Programme of the EU (SFERA 2 Grant Agreement no. 312643) is gratefully acknowledged for the access to solar reactors. The characterization of the materials was supported by the Transilvania University of Brasov scholarship for international mobilities.

References

[1] R. S. Oosthuizen and V. O. Nyamori, "Carbon nanotubes as supports for palladium and bimetallic catalysts for use in hydrogenation reactions," *Platinum Metals Review*, vol. 55, no. 3, pp. 154–169, 2011.

[2] T. Aruga, "Hydrogen absorption and hydrogenation by palladium," *Hyomen Kagaku*, vol. 27, no. 6, pp. 341–347, 2006.

[3] J. Muzart, "Palladium-catalysed oxidation of primary and secondary alcohols," *Tetrahedron*, vol. 59, no. 31, pp. 5789–5816, 2003.

[4] L. Wang, X. Chen, J. Liang, Y. Chen, X. Pu, and Z. Tong, "Kinetics of the catalytic isomerization and disproportionation of rosin over carbon-supported palladium," *Chemical Engineering Journal*, vol. 152, no. 1, pp. 242–250, 2009.

[5] E. Antolini, "Palladium in fuel cell catalysis," *Energy & Environmental Science*, vol. 2, no. 9, p. 915, 2009.

[6] J. Boon, V. Spallina, Y. van Delft, and M. van Sint Annaland, "Comparison of the efficiency of carbon dioxide capture by sorption-enhanced water-gas shift and palladium-based membranes for power and hydrogen production," *International Journal of Greenhouse Gas Control*, vol. 50, pp. 121–134, 2016.

[7] R. Pattabiraman, "Electrochemical investigations on carbon supported palladium catalysts," *Applied Catalysis A: General*, vol. 153, no. 1-2, pp. 9–20, 1997.

[8] R. Narayanan and M. A. El-Sayed, "Carbon-supported spherical palladium nanoparticles as potential recyclable catalysts for the Suzuki reaction," *Journal of Catalysis*, vol. 234, no. 2, pp. 348–355, 2005.

[9] L. Guo, J. Bai, J. Wang et al., "Fabricating series of controllable-porosity carbon nanofibers-based palladium nanoparticles catalyst with enhanced performances and reusability," *Journal of Molecular Catalysis A: Chemical*, vol. 400, pp. 95–103, 2015.

[10] Y.-M. Lu, H.-Z. Zhu, W.-G. Li, B. Hu, and S.-H. Yu, "Size-controllable palladium nanoparticles immobilized on carbon nanospheres for nitroaromatic hydrogenation," *Journal of Materials Chemistry A*, vol. 1, no. 11, pp. 3783–3788, 2013.

[11] R. M. Lago, S. C. Tsang, K. L. Lu, Y. K. Chen, and M. L. H. Green, "Filling carbon nanotubes with small palladium metal crystallites: the effect of surface acid groups," *Journal of the Chemical Society, Chemical Communications*, vol. 3, no. 13, p. 1355, 1995.

[12] X. Yang, Q. Li, H. Wang et al., "Green synthesis of palladium nanoparticles using broth of *Cinnamomum camphora* leaf," *Journal of Nanoparticle Research*, vol. 12, no. 5, pp. 1589–1598, 2010.

[13] A. J. Kora and L. Rastogi, "Green synthesis of palladium nanoparticles using gum ghatti (*Anogeissus latifolia*) and its application as an antioxidant and catalyst," *Arabian Journal of Chemistry*, pp. 0–9, 2015.

[14] A. Pascu, E. M. Stanciu, D. Savastru, V. Geanta, and C. Croitoru, "Optical and microstructure characterisation of ceramic-hydroxyapatite coating fabricated by laser cladding," *Journal of Optoelectronics and Advanced Materials*, vol. 19, pp. 66–72, 2017.

[15] G. Flamant, J. F. Robert, S. Marty et al., "Solar reactor scaling up: the fullerene synthesis case study," *Energy*, vol. 29, pp. 801–809, 2004.

[16] D. Negrea, C. Ducu, S. Moga et al., "Solar physical vapor deposition preparation and microstructural characterization of TiO_2 based nanophases for dye-sensitized solar cell applications," *Journal of Nanoscience and Nanotechnology*, vol. 12, no. 11, pp. 8746–8750, 2012.

[17] K. Smits, L. Grigorjeva, D. Millers et al., "Luminescence properties of zirconia nanocrystals prepared by solar physical vapor deposition," *Optical Materials*, vol. 37, pp. 251–256, 2014.

[18] I. Apostol, K. V. Saravanan, C. J. A. Monty, and P. M. Vilarinho, "Solar physical vapor deposition: a new approach for preparing magnesium titanate nanopowders," *Applied Surface Science*, vol. 285, pp. 49–55, 2013.

[19] D. Luxembourg, G. Flamant, and D. Laplaze, "Solar synthesis of single-walled carbon nanotubes at medium scale," *Carbon*, vol. 43, pp. 2302–2310, 2005.

[20] G. Flamant, D. Luxembourg, J. F. Robert, and D. Laplaze, "Optimizing fullerene synthesis in a 50 kW solar reactor," *Solar Energy*, vol. 77, no. 1, pp. 73–80, 2004.

[21] E. M. Stanciu, A. Pascu, I. C. Roata et al., "Solar radiation synthesis of functional carbonaceous materials using Al2O3/TiO2-Cu-HA doped catalyst," *Applied Surface Science*, 2017, in press.

[22] N. T. K. Thanh, N. Maclean, and S. Mahiddine, "Mechanisms of nucleation and growth of nanoparticles in solution," *Chemical Reviews*, vol. 114, no. 15, pp. 7610–7630, 2014.

[23] S. W. Kim, J. Park, Y. Jang et al., "Synthesis of monodisperse palladium nanoparticles," *Nano Letters*, vol. 3, no. 9, pp. 1289–1291, 2003.

[24] D. R. Lide, "CRC handbook of chemistry and physics, 84th edition, 2003-2004," *Handbook of Chemistry and Physics*, vol. 53, p. 2616, 2003.

[25] W. E. Vaughan and G. B. Kistiakowsky, "The heat of sublimation of carbon," *Physical Review*, vol. 40, pp. 457–462, 1932.

[26] C. L. Nehl, H. Liao, and J. H. Hafner, "Optical properties of star-shaped gold nanoparticles," *Nano Letters*, vol. 6, no. 4, pp. 683–688, 2006.

[27] M. Bystrzejewski, M. H. Rummeli, T. Gemming, H. Lange, and A. Huczko, "Catalyst-free synthesis of onion-like carbon nanoparticles," *New Carbon Materials*, vol. 25, no. 1, pp. 1–8, 2010.

[28] L. Stobinski, B. Lesiak, A. Malolepszy et al., "Graphene oxide and reduced graphene oxide studied by the XRD, TEM and electron spectroscopy methods," *Journal of Electron Spectroscopy and Related Phenomena*, vol. 195, pp. 145–154, 2014.

[29] S. Navaladian, B. Viswanathan, T. K. Varadarajan, and R. P. Viswanath, "A rapid synthesis of oriented palladium nanoparticles by UV irradiation," *Nanoscale Research Letters*, vol. 4, no. 2, pp. 181–186, 2009.

[30] N. Mohajeri, A. T-Raissi, G. Bokerman et al., "TEM-XRD analysis of PdO particles on TiO_2 support for chemochromic detection of hydrogen," *Sensors and Actuators B: Chemical*, vol. 144, no. 1, pp. 208–214, 2010.

[31] W. Vogel, "Interaction of a nanosized Pd catalyst with active C from the carbon support: an advanced in situ XRD study," *Journal of Physical Chemistry C*, vol. 115, no. 5, pp. 1506–1512, 2011.

[32] W. Lisowski, E. G. Keim, Z. Kaszkur, A. H. J. Van Den Berg, and M. A. Smithers, "Microstructural and chemical transformation of thin Ti/Pd and TiD y/Pd bilayer films induced by vacuum annealing," *Analytical and Bioanalytical Chemistry*, vol. 389, no. 5, pp. 1489–1498, 2007.

[33] A. Monshi, M. R. Foroughi, and M. R. Monshi, "Modified Scherrer equation to estimate more accurately nano-crystallite size using XRD," *World Journal of Nano Science and Engineering*, vol. 2, no. 3, pp. 154–160, 2012.